

Cyclic Policy Distillation: Sample-Efficient Sim-to-Real Reinforcement Learning with Domain Randomization

Yuki Kadokawa^{a,*}, Lingwei Zhu^a, Yoshihisa Tsurumine^a, Takamitsu Matsubara^a

^a*Graduate School of Science and Technology, Division of Information Science, Nara Institute of Science and Technology, 8916-5 Takayamacho, Ikoma, Nara, Japan*

Abstract

Deep reinforcement learning with domain randomization learns a control policy in various simulations with randomized physical and sensor model parameters to become transferable to the real world in a zero-shot setting. However, a huge number of samples are often required to learn an effective policy when the range of randomized parameters is extensive due to the instability of policy updates. To alleviate this problem, we propose a sample-efficient method named Cyclic Policy Distillation (CPD). CPD divides the range of randomized parameters into several small sub-domains and assigns a local policy to each sub-domain. Then, the learning of local policies is performed while *cyclically* transitioning the target sub-domain to neighboring sub-domains and exploiting the learned values/policies of the neighbor sub-domains with a monotonic policy-improvement scheme. Finally, all of the learned local policies are distilled into a global policy for sim-to-real transfer. The effectiveness and sample efficiency of CPD are demonstrated through simulations with four tasks (Pendulum from OpenAIGym and Pusher, Swimmer, and HalfCheetah from Mujoco), and a real-robot ball-dispersal task.

Keywords: domain randomization, sim-to-real, deep reinforcement learning

2020 MSC: 00-01, 99-00

*Corresponding author

Email addresses: `kadokawa.yuki.kv3@is.naist.jp` (Yuki Kadokawa), `zhu.lingwei.zj5@is.naist.jp` (Lingwei Zhu), `tsurumine.yoshihisa@is.naist.jp` (Yoshihisa Tsurumine), `takam-m@is.naist.jp` (Takamitsu Matsubara)

1. Introduction

Deep reinforcement learning (DRL) is one of the most promising methods for robots to automatically acquire autonomous control policies through interaction with a real-world environment [1, 2, 3]. Recent studies utilize DRL to learn control policies in simulation with randomized physical and sensor model parameters and thus make these policies transferable to the real world in a zero-shot setting [4, 5, 6]. Such use of RL with Domain Randomization (DR) is attractive because it can avoid robot failure or very long-time learning in the real world; however, it often requires a huge number of samples due to the instability of policy updates caused by unstable policy gradients [7, 8].

Sample efficiency, evaluated by the number of samples required to reach a certain performance threshold, is one of the biggest subjects for DRL. Existing methods on improving sample efficiency fall into two categories: limiting the range of randomized parameters [9, 10, 11]; or dividing the full domain into several sub-domains and learns *local policies* restricted to each of the sub-domain [12, 7, 13]. Both categories suffer from issues such as the lack of real-world samples for a posteriori adjusting the ranges, or the inefficiency resulted from independence between sub-domains.

Consequently, if there were a mechanism to share samples or learned values/policies among sub-domains, it might be possible to improve sample efficiency. Nevertheless, naïvely sharing may even degrade the performance due to domain gaps between sub-domains. Therefore, we are motivated to develop a new scheme that appropriately shares learned values/policies among sub-domains to improve both sample efficiency and learning performance. Specifically, if the sub-domains share similar parameters, the resulting MDPs might also resemble. Under this assumption, the values/policies in the similar sub-domains may share similar characteristics. Therefore, we hypothesize that learning could be accelerated by transferring among neighboring partitioned sub-domain’s values/policies. This assumption will be validated empirically

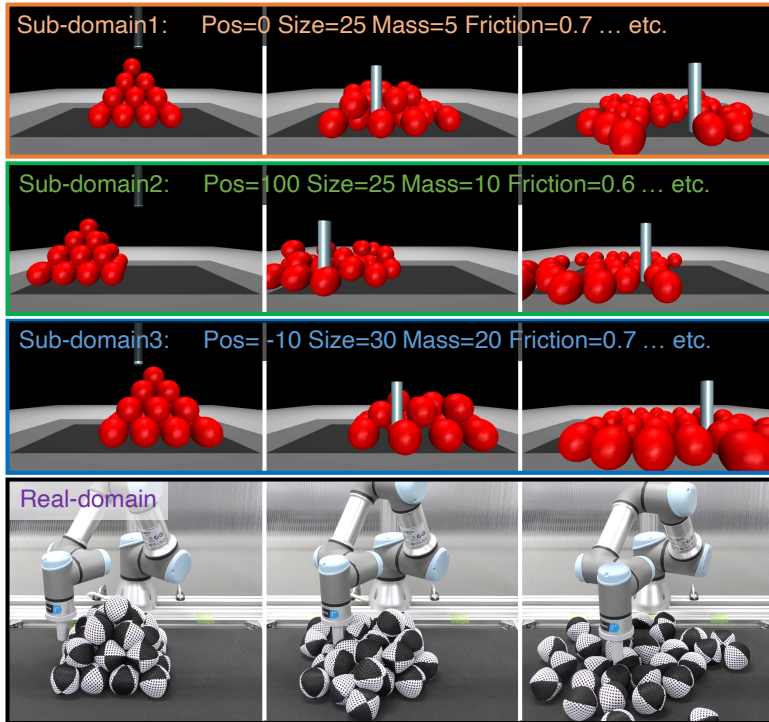


Figure 1: Experimental scenes of the robotic ball-dispersal task with domain randomization: Upper three rows are simulation environments; bottom row is the real-world environment. Simulation parameters such as ball size (radius) and ball-position (center position of all balls) are randomized. Sub-domains are made from a simulation environment formed by dividing the range of randomized parameters. Learned policies in all sub-domains are distilled into a global policy to be transferred to a real domain for sim-to-real transfer.

through our experiments.

This paper proposes Cyclic Policy Distillation (CPD) as a sample efficient RL method for sim-to-real in the zero-shot setting. CPD divides the range of randomized parameters into several small sub-domains and assigns a local policy to each sub-domain. Then, the learning of local policies is performed while *cyclically* transitioning the target sub-domain to neighboring sub-domains and the learned values/policies of the neighboring sub-domains are exploited with a monotonic policy-improvement scheme. Finally, all of the learned local policies are distilled into a global policy for sim-to-real transfer. To validate the effectiveness and sample efficiency of CPD, we evaluated it on simulation prob-

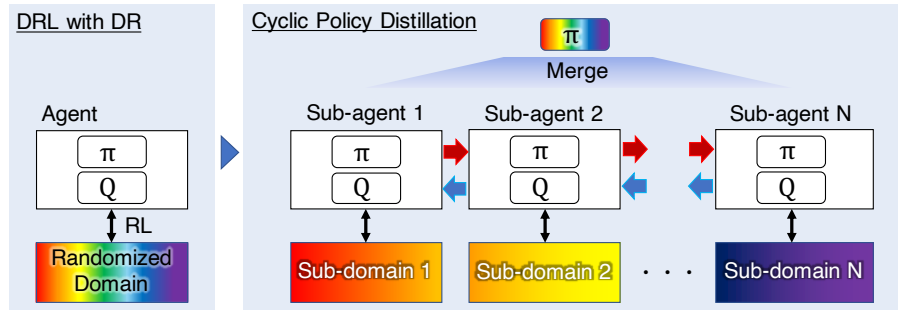


Figure 2: Overview of Cyclic Policy Distillation: Unlike typical methods that conduct DR in simulations with the full range of randomized parameters, CPD divides the range of randomizing parameters into several small sub-domains and assigns a local policy to each sub-domain. Then, the learning of local policies is performed while *cyclically* transitioning the target sub-domain to neighboring sub-domains and exploiting the learned values/policies of the neighboring sub-domains with a monotonic policy-improvement scheme. Finally, all of the learned local policies are distilled into one global policy for sim-to-real transfer.

lems, i.e., with four tasks (Pendulum from OpenAIGym [14] and Pusher, Swimmer, and HalfCheetah from Mujoco [15]), and a real-robot ball-dispersal task (Fig. 1). The ball-dispersal task is designed as a simplified environment for operations that handle multiple particulate objects, such as powder manipulation [16, 17, 18] and soil excavation [19, 20, 21]. The simplification is achieved by using the increased ball size with the small number of balls; however, its difficulties of applying DRL due to the hardness of automatic initialization and the enormous patterns of observation samples with their irregular shape and deformations remain. Therefore, it is a suitable task to be tackled by a sim-to-real approach.

The rest of this paper is organized as follows. Sec. 2 states related works. In Sec. 3, we offer preliminary considerations before discussing the proposed method, and Sec. 4 describes the proposed CPD method. Sec. 5 presents simulation experiments, while Sec. 6 presents real-robot experiments. In Sec. 7, we discuss limitations of the CPD method. Finally, Sec. 8 concludes this paper.

2. Related Works

2.1. *Distilling Multiple Policies into a Single Policy*

Policy Distillation (PD) [22] for integrating multiple policies into a single policy is used in the proposed CPD method and in previous works as described in Sec. 2.2. Modern deep learning features large-scale models that contain millions of parameters. A significant portion of those parameters may actually be redundant, thus contributing little to the final learned performance. Hence, it is advantageous to compress large-scale models into smaller ones to save computational resources without degrading performance. Motivated by the need for compression, the core function of PD is to express the knowledge of a large policy network via a much smaller one [22, 23]. Besides compressing purpose, PD has natural applications in multi-task RL, where the policies learned in each of the sub-tasks are merged into a single policy to achieve comparable performance on all sub-tasks [24, 25, 26]. In this paper, the proposed method performs these two distillation tasks to transfer learned knowledge between local policies in divided sub-domains, followed by the final integration of all local policies into a single global policy.

2.2. *Dividing Range of Randomized Parameters*

In the zero-shot settings of RL with DR, some studies have attempted to stabilize the learning process. Specifically, when DR frequently switches the randomized parameters, there is considerable variation in the samples, and the updating direction of the policies can also frequently change. Thus, the learning of the policies becomes unstable, resulting in low sample efficiency and poor performance [7]. Previous works have stabilized the updating policies by dividing the range of randomized parameters into smaller ranges to avoid frequent changes in the policies. For this purpose, the following four major approaches have been pursued.

Distilled Domain Randomization (DiDoR) [12]: In this approach, the learning of local policies and their generalization to global policy are performed

Method	DiDoR	P2PDRL	DnC	BS	CPD
Dist. /Partition	✓	✓	✓	-	✓
Know.-trans.	-	✓	✓	-	✓
Range-adjust	-	-	-	✓	-
Scheduling	-	-	-	-	✓

Table 1: Characteristics of proposed method and related works: Dist. /Partition means the methods using policy distillation and partitioning parameters, Know.-trans. means the methods learning local policies/values with transferring knowledge between local policies/values, Range-adjust means the methods optimizing the parameter distribution, Scheduling means the methods learning local policies/values with scheduled transitions of sub-domains.

separately. First, each local policy is learned independently. After the learning of all local policies have converged, the policies are distilled into a single global policy.

Peer-to-Peer Distillation Reinforcement Learning (P2PDRL) [7]:

In this approach, local policies are learned and generalized simultaneously to a single global policy. After a certain number of learning iterations with generalization of distilling each local policy, all of the local policies change their learning range of randomized parameters. By repeating this process, the local policies gradually become a global policy that works in all ranges of randomized parameters.

Divide-and-Conquer (DnC) [13]: This approach alternates between learning local policies and generalizing them to a single global policy. After all of the local policies have been learned for a certain number of samples, they are distilled into the global policy for generalization. These procedures are repeated until the learning converges.

BayesSim (BS) [11]: This approach performs test behaviors in a real-world environment using the policies obtained in the simulation. The range of randomized parameters is shifted and limited by a probabilistic distribution so that it cover the plausible parameters based on the errors between state-action sequences in simulation and in the real world. Thus, executing actions in the real-world is necessary, and is outside the scope of this paper, which aims for a zero-shot setup.

A common feature of the above previous methods, except BayesSim, is that the sub-domains to be learned are selected *randomly*. Therefore, the gap of sub-domains in distillation can be large, making the learning results unstable and failing to improve the sample efficiency. In contrast to these methods, our proposed method *cyclically* transitions to neighboring sub-domains with similar ranges of randomized parameters and exploits the neighboring sub-domains’ learned values/policies with a monotonic policy-improvement scheme. Consequently, values/policies are shared within small-gap domains to ensure improved learning stability and sample efficiency. Characteristics of our proposed method and related works are summarized in Table 1.

3. Preliminaries

3.1. Reinforcement Learning with Domain Randomization

Reinforcement Learning (RL) problems are typically formulated by Markov Decision Processes (MDP) expressed by the components $(\mathcal{S}, \mathcal{A}, \mu, \mathcal{P}, r, \gamma)$. \mathcal{S} is the set of observations that can be obtained from the environment, and \mathcal{A} is the set of selectable actions. μ is the initial state distribution. $\mathcal{P}_{ss'}^a$ denotes the probability of transitioning to observation $s' \in \mathcal{S}$ when action $a \in \mathcal{A}$ is chosen, given observation $s \in \mathcal{S}$. The reward for making the transition is represented by $r_{ss'}^a$, and $\gamma \in [0, 1)$ is the discount factor. Policy $\pi(a|s)$ is the probability of choosing action a given s . We define the stationary distribution induced by π as $d_{\pi, \mu}(s) = (1 - \gamma) \sum_{t=0}^{\infty} \gamma^t \mathcal{P}(s_t = s | \mu, \pi)$.

For each observation s , the evaluation criterion V^π under the policy π can be defined:

$$V^\pi(s) = \mathbb{E}_{\pi, \mathcal{P}} \left[\sum_{t=0}^{\infty} \gamma^t r_{s_t} \mid s_0 = s \right], \quad (1)$$

where $r_{s_t} = \sum_{\substack{a_t \in \mathcal{A} \\ s_{t+1} \in \mathcal{S}}} \pi(a_t | s_t) \mathcal{P}_{s_t s_{t+1}}^{a_t} r_{s_t s_{t+1}}^{a_t}$. The goal of RL is to find an optimal policy π^* that maximizes the discounted total reward starting from arbitrary initial observation s_0 drawn from μ : $J_\mu^{\pi^*} = \sum_{s_0} d_{\pi^*, \mu}(s_0) V^*(s_0)$. It is a well

known result that such an optimal policy satisfies the Bellman equation:

$$V^*(s) = \max_{\pi} \sum_{a \in \mathcal{A}, s' \in \mathcal{S}} \pi(a|s) \mathcal{P}_{ss'}^a (r_{ss'}^a + \gamma V^*(s')), \quad (2)$$

where $V^*(s)$ is the optimal value function. To evaluate policies based not only on observation s but also action a , the optimal value function is defined:

$$Q^*(s, a) = \max_{\pi} \sum_{s' \in \mathcal{S}} \mathcal{P}_{ss'}^a (r_{ss'}^a + \gamma \sum_{a' \in \mathcal{A}} \pi(a'|s') Q^*(s', a')). \quad (3)$$

Given a Q , we can extract its greedy policy by the greedy operator $\mathcal{G}(Q^\pi) := \operatorname{argmax}_{\pi} Q^\pi(s, a)$. The relationships of Eqs. (2) and (3) hold also for arbitrary stationary policy π by removing the max operator. We also define advantage function $A^\pi(s, a) = Q^\pi(s, a) - V^\pi(s)$ as the evaluation of how well an action performs compared to the average. The expected advantage can be defined as the expectation of $A^\pi(s, a)$ w.r.t. another policy π' : $A_{\pi'}^\pi(s) = \sum_a \pi'(a|s) A_\pi(s, a)$.

As for RL with DR, the transition probability depends on domain-specific parameter. Then, suppose that there are N randomly sampled domains each of which has its own specific transition probability as $\mathcal{P}_{ss'}^{a,(n)}$ where $n \in N$. The goal of RL with DR is to find an optimal policy π^* that *commonly* maximizes the following equation for all N domains:

$$Q^{*,(n)}(s, a) = \max_{\pi} \sum_{s' \in \mathcal{S}} \mathcal{P}_{ss'}^{a,(n)} (r_{ss'}^a + \gamma \sum_{a' \in \mathcal{A}} \pi(a'|s') Q^{*,(n)}(s', a')), \quad (4)$$

where all domains share the same reward function. Each domain possesses its own policy and value function.

3.2. Monotonic Policy Improvement in RL

In the presence of various errors and noises such as approximation error and observation noise, there is no guarantee that the updated RL policy can achieve improved performance. Degraded performance could pose a threat to physical systems like robots.

Drawing inspiration from the classic but popular monotonic improvement (MI) literature [27, 28, 29], the problem of performance degradation can be solved if one can ensure that the updated policy π_{k+1} attains non-negative improvement Δ_{k+1} against π_k , i.e. $J_{\mu}^{\pi_{k+1}} - J_{\mu}^{\pi_k} \geq \Delta_{k+1} \geq 0$. Conservative Policy Iteration (CPI) [27] is one such method that guarantees lower-bounded improvement $\Delta_{k+1} \geq 0$ by linearly interpolating the current policy and the greedy policy:

$$\pi_{k+1} \leftarrow (1 - m_{k+1})\pi_k + m_{k+1}\mathcal{G}(Q^{\pi}), \quad (5)$$

where $m_{k+1} \in [0, 1]$ is the policy mixture rate. It has been shown that the policy improvement lower bound Δ_{k+1} is a negative quadratic function in m_{k+1} [27], hence we can solve for the maximizer m_{k+1}^* :

$$m_{k+1}^* = \frac{1 - \gamma}{4R} \sum_{s \in \mathcal{S}} d_{\pi_k, \mu}(s) \sum_{a \in \mathcal{A}} \pi_{k+1}(a|s) A^{\pi_k}(s, a), \quad (6)$$

where R is the maximum possible reward.

4. Cyclic Policy Distillation

To alleviate the sample inefficiency of RL with DR, we propose a sample-efficient method named Cyclic Policy Distillation (CPD). An overview of CPD is shown in Fig. 2. Specifically, CPD consists of the following three steps:

1. Dividing the randomized domain into sub-domains.
2. Cyclic learning of all local policies.
3. Distilling local policies into a single global policy.

Details of these steps are described below, with pseudo-code provided in Algorithm 1.

4.1. Dividing Randomized Domain into Sub-domains

CPD divides the range of randomized parameters into sub-domains and assigns a local policy to each sub-domain. To this end, we set target parameters

Algorithm 1: Cyclic Policy Distillation

```
# Set parameters described in Table 2
# Separate the domain to sub-domains into  $N$ 
# Set networks of policies and value functions
# Set replay buffers  $\mathcal{D}$  of sub-domains
while until converge do
  for  $n = 1, 2, \dots, N, N, N - 1, \dots, 1$  do
    for  $e = 1, 2, \dots, E$  do
      for  $t = 1, 2, \dots, T$  do
        # Get observation  $s_t^{(n)}$ , reward  $r^{(n)}$ 
        # Take action  $a_t^{(n)}$  with policy  $\pi^{(n)}$ 
        # Push  $(s_t^{(n)}, a_t^{(n)}, r^{(n)})$  to  $\mathcal{D}^{(n)}$ 
        # Update value function  $Q^{(n)}$  by RL
        # Update policy  $\pi^{(n)}$  by Eq. (8)
      # Copy network parameters of  $Q^{(n)}$  to next sub-domain's  $Q$ 
  while until converge do
    for  $n = 1, 2, \dots, N$  do
      for  $t = 1, 2, \dots, T$  do
        # Get observation  $s_g^{(n)}$ 
        # Take action  $a_g^{(n)}$  with policy  $\pi^{(g)}$ 
        # Push  $(s_g^{(n)}, a_g^{(n)})$  to  $\mathcal{D}^{(g)}$ 
        # Distill policy  $\pi^{(g)}$  with  $\pi^{(n)}$  by Eq. (9)
```

and their randomization ranges and divide them into N parts, each of which is utilized as the randomization range of each sub-domain. The sub-domains with adjacent index numbers $n \in \{1, \dots, N\}$ should be set up so that their randomization ranges are *similar*, which is a key arrangement for subsequent steps of CPD as explained later.

The number of divisions N can be arbitrarily defined; however, there may be a trade-off between sample efficiency and stability since a small N makes the range of each sub-domain large and thus causes unstable learning, and vice versa.

4.2. Cyclic Learning of All Local Policies

For each sub-domain, we define its sub-agent including local policy $\pi^{(n)}$ and local value function $Q^{(n)}$, where n is an index of the sub-domain. Then, the

Para.	Meaning	Value
N	Domain division number (Pendulum)	4
	Domain division number (the others)	6
m_0	Coefficient of MI	1
γ	Discount factor of RL	0.99
E	Number of episodes per domain-shift	15
B	Minibatch size (number of episodes)	16
T	Number of steps per episode	150

Table 2: Learning parameters of CPD in experiments.

learning of local policies is performed while *cyclically* transitioning the target sub-domain to neighboring sub-domains, and the learned values/policies of the neighboring sub-domains are exploited with a monotonic policy-improvement scheme [27, 28, 29]. The details of the flow of the learning process are described below.

4.2.1. Execution Flow

At the first step, the previous sub-domain’s local value function $Q^{(n-1)}$ is copied to that of the current sub-domain $Q^{(n)}$. Then at each time step t , the local value function $Q^{(n)}$ and local policy $\pi^{(n)}$ are updated by RL through interaction with the current sub-domain. To accelerate local policy learning, we apply the monotonic policy-improvement scheme [27, 28, 29] based on the similarity between the neighboring sub-domains as assumed in the domain division step. Specifically, the linear mixture composition of the neighboring local policy $\pi^{(n-1)}$ and the updating current local policy $\pi^{(n)}$ is considered (its details are given in the following subsection). After training in the current sub-domain for a certain number of episodes, the learning sub-domain proceeds to the next one $n+1$. The above explanation regards the forward transition starting from $n = 0$ to $n = N$; then, it switches to the backward transition starting from $n = N$ to 0. These are iterated repeatably until the learning is converged.

4.2.2. Policy Mixing

CPD approximately utilizes the MI scheme in Eq. (5) for accelerating the learning of local policy $\pi_k^{(n)}$ by appropriately exploiting neighboring sub-domain local policy $\pi^{(n')}$. This “approximation” will be accurate if the range of randomization parameters of neighboring sub-domains are similar; otherwise, it will be coarse due to the domain gap. The original coefficient computation scheme in Eq. (6) requires knowledge of the maximum reward and stationary distribution $d_{\pi, \mu}$, which is seldom possible in practice. Therefore, we will implement it by utilizing recent studies [30, 31] that have been shown to work well experimentally. As a result, we extend Eqs. (5) and (6) as follows:

$$\begin{cases} m_{k+1} = m_0 \mathbb{E}_{s \sim \mathcal{D}^{(n)}} [\mathbb{E}_{a' \sim \pi^{(n')}} [Q_{k+1}^{(n)}(s, a')] \\ \quad - \mathbb{E}_{a \sim \pi_k^{(n)}} [Q_{k+1}^{(n)}(s, a)]], \\ \pi_{k+1}^{(n)} \leftarrow (1 - m_{k+1})\pi_k^{(n)} + m_{k+1}\pi^{(n')}, \end{cases} \quad (7)$$

where m_0 is a constant coefficient, $\mathcal{D}^{(n)}$ is the replay buffer of the current sub-domain, and k is an update number. Thus, the overall loss function of updating local policies \mathcal{L} for learning the local policy $\pi_k^{(n)}$ is defined:

$$\begin{cases} \mathcal{L}_{\pi^{(n)}}^{\text{MI}}(\theta^{(n)}) = \text{KL}(\pi_{\theta^{(n)}}^{(n)} \parallel (1 - m)\pi_{\theta^{(n)}}^{(n)} + m\pi_{\theta^{(n')}}^{(n')}), \\ \mathcal{L}_{\pi^{(n)}}(\theta^{(n)}) = \mathcal{L}_{\pi^{(n)}}^{\text{RL}}(\theta^{(n)}) + \mathcal{L}_{\pi^{(n)}}^{\text{MI}}(\theta^{(n)}), \end{cases} \quad (8)$$

where $\theta^{(n)}$ is network parameters of local policies, \mathcal{L}^{RL} is an RL loss function, and \mathcal{L}^{MI} is a loss function estimated from Eq. (7).

4.3. Global Distillation

At the end of sub-domain learning, the local policies $\pi^{(n)}$ are distilled into the single global policy $\pi^{(g)}$, which stands in contrast to prior work that learns both the local policies and the global one simultaneously [7, 13]. These works distill incomplete local policies that are still in the learning process, and updating global policies repeatedly with local policy actions that have low reward

Pendulum	Rate	Mujoco	Rate
Gravity	[0.7, 1.5]	Gravity	[0.5, 2]
Timestep	[0.8, 1.2]	Timestep	[0.5, 2]
Bar-mass	[0.8, 1.2]	Friction	[0.5, 2]
Bar-length	[0.8, 1.2]	Mass	[0.5, 2]
Actuator-gain	[0.7, 1.5]	Actuator-gain	[0.5, 2]
Actuator-bias	[-0.5, 0.5]	Actuator-damping	[0.5, 2]

Table 3: Range of randomized parameters of (**Left**) Pendulum and (**Right**) Mujoco environments.

leads to increased learning time. Thus, in CPD, learning of global policy is explicitly done only in this process after completing the learning of individual local policies.

The flow of this process is given below, where the aim is to learn a global policy $\pi^{(g)}$ that has similar performance to those of the local policies $\pi^{(n)}$ for their respective domains. Specifically, we loop over the following three steps until convergence or the maximum number of iterations is reached: (1) Obtain rollout $(s_{g,t}^{(n)}, a_{g,t}^{(n)}, r_{g,t}^{(n)}, s_{g,t+1}^{(n)}, a_{g,t+1}^{(n)})$ in each sub-domain n using $\pi^{(g)}$, since it is more sample-efficient than rollout by local policies $\pi^{(n)}$ (reason described in [32]). (2) Evaluate the learned local policy action probability from the observation $s_g^{(n)}$. (3) Distill the global policy $\pi^{(g)}$ with the local policy action $a^{(n)}$. The above flow can be executed by optimizing the following loss function:

$$\mathcal{L}_{\pi^{(g)}}(\theta) = \sum_n \mathbb{E}_{s_g^{(n)}, a_g^{(n)} \sim \mathcal{D}^{(g)}} \left[\text{KL}(\pi^{(g)}(s_g^{(n)}, a_g^{(n)}) || \pi^{(n)}(s_g^{(n)}, a_g^{(n)})) \right]. \quad (9)$$

5. Simulation Experiment

In this section, we validate the performance of the proposed CPD method in simulation. Specifically, we investigate the following:

1. Effect of the exploitation of neighboring local policies and copying of the

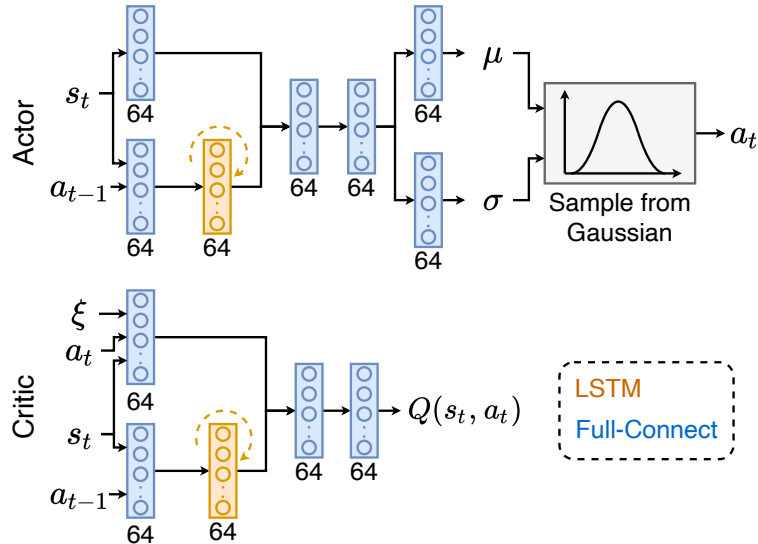


Figure 3: Network structure of CPD in experiment: CPD use an actor-critic structure. The actor have policy-network output continues action a_t by estimating mean μ and standard deviation σ of the Gaussian distribution used for sampling actions a_t . The critic has a value network that evaluates value function Q , whose inputs contain domain parameters ξ . These networks consist of fully connected layers and LSTM layers with 64 nodes.

local value functions for faster learning in CPD (Sec. 5.2);

2. Effect of the number and method of divisions of domain decomposition in CPD on learning stability and convergence (Sec. 5.3);
3. Comparison of proposed CPD method with previous works and ablation methods (Sec. 5.4)

5.1. Common Settings

We leverage Soft Actor-Critic (SAC) [33] as the base algorithm for implementing CPD. and select four tasks: OpenAI Gym Pendulum, Pusher, Swimmer, and HalfCheetah from Mujoco. The randomization settings of the domain parameters are shown in Table 3. CPD has LSTM layers in both the actor network and critic network because it is virtually not possible to distinguish dynamical parameters without a recurrent network architecture or more general a history of states and actions. The network architecture of CPD is shown in Fig. 3. CPD has LSTM layers in both the actor network and critic network

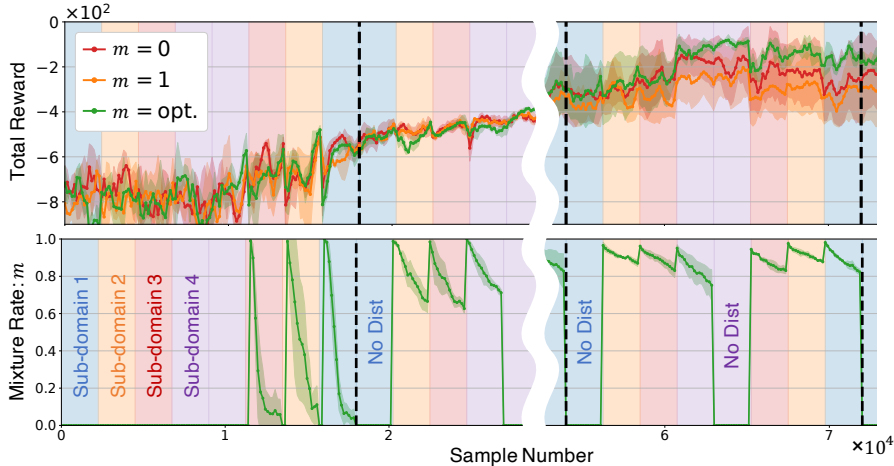


Figure 4: Learning curves (top) and policy mixture rate (bottom): CPD divides the range of randomized parameters into four sub-domains, indicated by light-colored regions of sub-domain1: blue, sub-domain2: orange, sub-domain3: red, sub-domain4: purple. The CPD learns in each sub-domain and cyclically changes sub-domains by (1) forward transition and (2) backward transition. Dashed line indicates one cycle of (1) and (2). No Dist means that the first sub-domains of (1) and (2) are not distilled by neighboring local policies because the distillations are not efficient due to the neighboring policies already utilized just previously. m means policy mixture rate, which is dynamically updated only in $m = \text{opt.}$. We started evaluating mixing rate m with 120 samples because the updating of local policies start from that number. Each curve is a plot of the mean and variance per sample of the five experiments.

because it is virtually not possible to distinguish dynamical parameters without a recurrent network architecture or more general a history of states and actions [34].

The actor network outputs the mean μ and standard deviation σ for a Gaussian distribution, from which the action a_t is sampled.

We implement previous methods with the following setup for fair comparison: (1) we change the base algorithm from Proximal Policy Optimization [35] to SAC, (2) we scale down the number of sample steps per episode due to the better sample efficiency of SAC, (3) we divide the domains same as CPD.

5.2. Effect of Updating Local Policies by Mixing

5.2.1. Settings

CPD accelerates local policy learning by exploiting neighboring local policies to mix the current local policies by the policy mixture rate m of Eq. (4). To

evaluate the effectiveness of the mixing rate, we compared its performance with other baselines with constant $m = 0$ or 1 for OpenAIGym Pendulum. $m = 0$ means neighboring local policies are not exploited for learning, and $m = 1$ means neighboring local policies are copied. $m = \text{opt.}$ means optimizing m by local value functions for stable acceleration of local policy learning.

5.2.2. Results

The results are shown in Fig. 4. From the total reward of Fig. 4, $m = \text{opt.}$ has the best sample efficiency and a 10 % higher final performance than the others. Furthermore, the performance of $m = 0$, with no acceleration by exploiting neighboring local policies, is better than $m = 1$, where neighboring local policies are exploited without optimization. These results shows that naively exploiting neighboring local policies, i.e., $m = 1$, is not always practical, perhaps due to the domain gaps. In fact, performance can be worse than without this exploitation.

From the transition of policy mixture rate m in CPD shown in Fig. 4, m tends to be low in the early stages of learning. This indicates that exploiting neighboring local policies in the initial stage is ineffective because they are nearly random policies. As the learning progresses, the local policies become more informative, and the mixing rate gains a larger quantity. Several instances where m rises sharply at a certain period correspond to the sub-domain transitions’ timing. As long as the learning sub-domain is fixed, m decays almost monotonically, indicating that it is beneficial to smoothly shift toward using samples from the current sub-domain for better policy improvement.

5.3. Evaluation of Number and Method of Divided Ranges

5.3.1. Settings

Since CPD divides the range of randomized parameters into N sub-domains for learning local policies, N and the partitioning method may influence the final performance and sample efficiency. Thus, we investigate the performance of CPD with various N and partitioning methods on Pendulum.

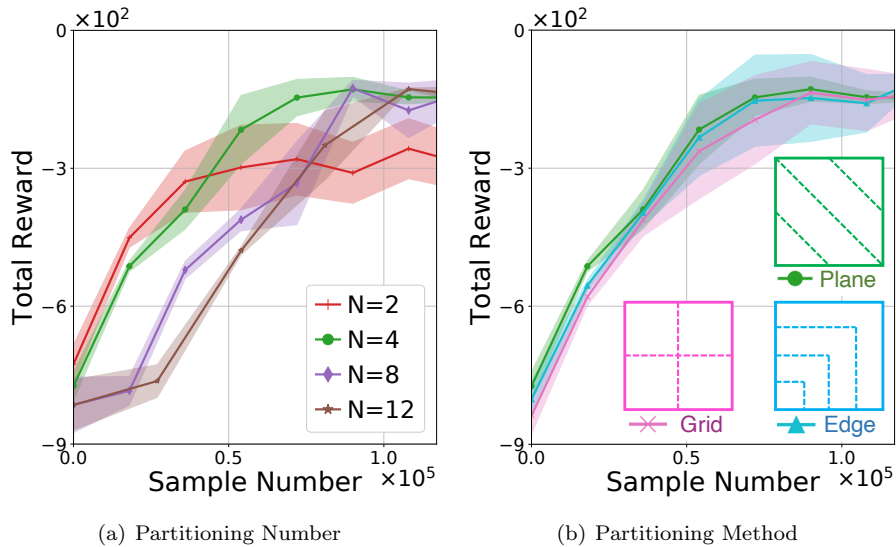


Figure 5: Performance comparison for (a) different numbers of partitions of the randomized parameter range (b) different patterns of partitioning methods: Partitioning methods are evaluated in three types, Plane, Edge, and Grid, as shown in (b). These outer lines indicate the entire range of parameters. The vertical and horizontal ranges each indicate the value of one parameter. The dashed lines indicate how to divide the parameters. All results of the partitioning method are evaluated in splitting four. Each curve of (a) and (b) plots the mean and variance per sample over five experiments.

5.3.2. Results

As shown in Fig. 5(a), it is visible that the highest performance and lowest sample efficiency happened when $N = 12$, i.e., the maximum number of sub-domains. On the other hand, the pair of lowest performance and highest sample efficiency occurred when $N = 2$, the minimum possible of divisions. The results indicate there is a trade-off in N between final performance and sample efficiency. The optimal balance is found at $N = 4$, and increasing N above that value gradually decreases sample efficiency.

As for the partitioning method shown in Fig. 5(b), the proposed method is robust to the patterns of partitioning methods in terms of total reward and sample efficiency. Based on this result, all subsequent experiments are evaluated by the “Plane”.

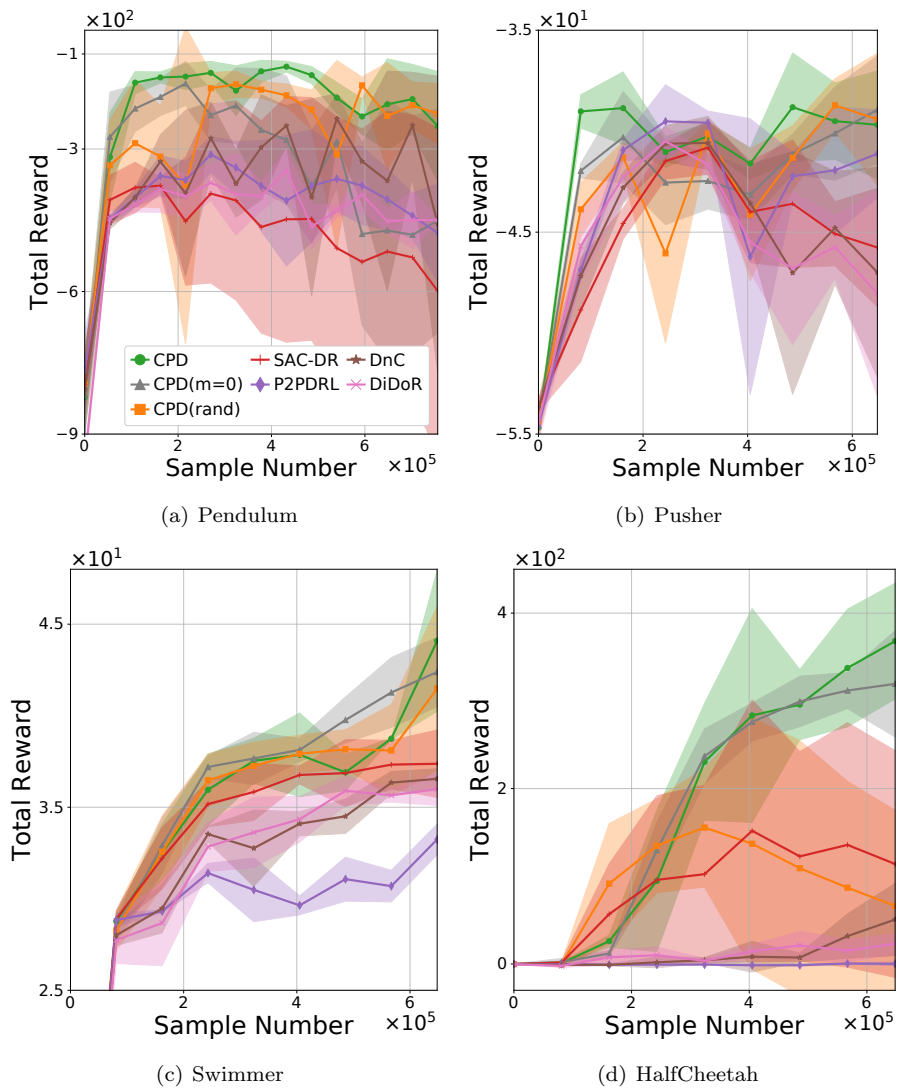


Figure 6: Learning curves of (a) Pendulum and (b) Pusher (c) Swimmer (d) HalfCheetah for different methods: SAC-DR is SAC using single-policy learning with DR, while P2PDRL, DnC and DiDoR are multiple-policy learning methods with the range of randomized parameters divided as described in Sec. 2.2. Moreover, CPD, CPD ($m = 0$), and CPD (rand) indicate CPD with full components, CPD without exploiting neighboring local policies, and CPD with random transitioning of sub-domains, respectively. Each curve plots mean and variance over five experiments.

5.4. Comparison with Other Methods

5.4.1. Settings

We compared the performance of CPD to other methods. We conducted the experiments with four environment: Pendulum, Pusher, Swimmer, and HalfCheetah.

5.4.2. Results

As shown in Fig. 6(a), CPD shows the highest performance by achieving a six-times and three-times better sample efficiency than the methods which achieve the best performance over all other methods. SAC, P2PDRL and DiDoR only achieved a low total reward that was under 70% of CPD. As shown in Fig. 6(d), none of the methods except CPD learned effective policies with a practical number of samples. SAC-DR, which does not partition the range of randomization parameters, learns quickly; however, the highest total reward is only about 40% of CPD. Moreover, as for the other environments shown in Fig. 6(b) and Fig. 6(c), CPD achieved the highest total reward and sample efficiency.

As an ablation study, we also applied CPD ($m = 0$) and CPD (rand). For Pendulum, CPD achieved about three-times better sample efficiency than CPD ($m = 0$), reaching the maximum total reward of CPD ($m = 0$). However, CPD ($m = 0$) has a significant performance degradation after learning convergence. Furthermore, CPD (rand) showed less sample efficiency than CPD ($m = 0$).

In summary, our comparisons to the previous works show the higher sample efficiency of the proposed method, and ablation studies show the effectiveness of the proposed architecture with the monotonic policy-improvement scheme and neighboring transitions of the sub-domain.

6. Real-Robot Experiment

In this section, we verify the effectiveness of the proposed method, CPD, on the ball-dispersal task as a real-world task (Fig. 1). The upper three rows

Physical	min	max	Observation	min	max
Gravity [m/s ²]	9	11	\mathbf{X}_{bias} [mm]	-10	10
Friction-coeff. [.]	0.6	1	\mathbf{Y}_{bias} [mm]	-10	10
Ball-mass [g]	5	20	\mathbf{Z}_{bias} [mm]	0	10
Ball-place [mm]	-125	125	$\mathbf{Z}_{\text{weight}}$ [.]	0.7	1.3
Ball-radius [mm]	25	30			

Table 4: Range of randomized parameters in the ball-dispersal task: Ball-place means the center position of the piled balls. When true ball-position is (x, y, z) , randomized positions are $(x + X_{\text{bias}}, y + Y_{\text{bias}}, z \times Z_{\text{weight}} + Z_{\text{bias}})$.

show the randomized simulation environment, and the bottom row shows the real-world environment. As shown in Fig. 1, this task is characterized by the countless ball-placement patterns that are possible in the process of collapsing a pile consisting of multiple balls. Thus, it is necessary for the agent to effectively learn an effective policy that can manage such innumerable ball patterns. In addition, this task is appropriate for a sim-to-real approach because it requires that the balls be restacked each time and that many initializations be made in the real robot environment.

6.1. Settings

The settings of the real-robot experiment are shown in Fig. 7. Given the depth image s^{depth} obtained from the depth camera mounted above the robot and the 3D coordinates s^{position} of the robot hand, the observation is defined as $s = [\text{Conv}(\text{Conv}(s^{\text{depth}})), s^{\text{position}}]$. The robot initializes the robot’s position for each action a to obtain the balls’ depth image without occlusion. The rotation of the robot hand is fixed so that it always faces the floor. Conv is a convolution operation with a kernel size of 3. s^{depth} compresses the number of pixels from [480, 640] to [5, 9]. s^{depth} is visualized in the second and fourth lines of Fig. 9. Action a is used to specify the robot’s fingertip in 3D relative coordinates and move it from the coordinates of the previous action. The distance that can be moved in one action is limited to 30 mm for each coordinate axis. Reward r is determined from the balls’ height to evaluate the collapse of the balls. The

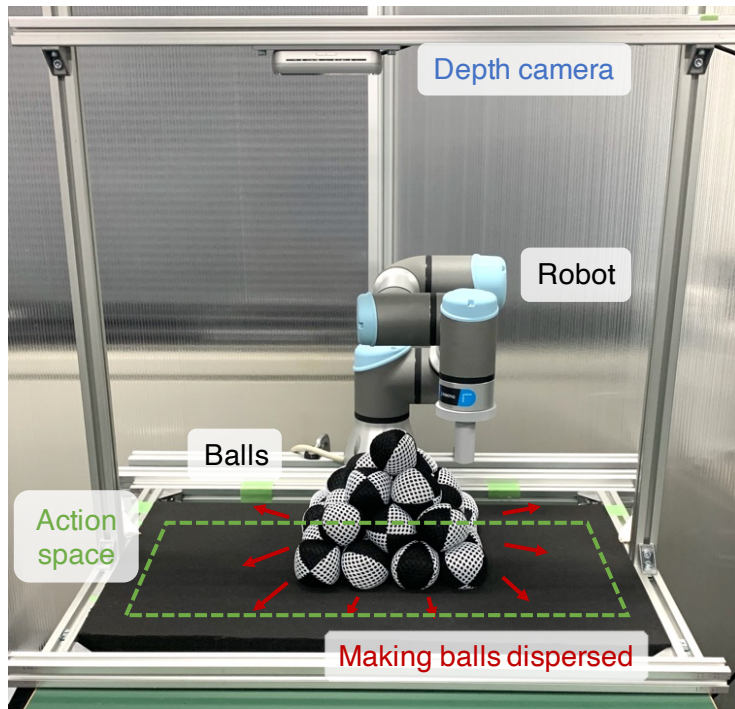


Figure 7: Experiment settings: This experiment uses UR3, and the task goal is to make the balls dispersed by the robot hand. The robot hand can move in the action space shown as a green dashed line. The depth camera captures the action space for getting observations.

number of balls is $B = 30$, and the reward is $r = \sum_{b=1}^B -h_i$, where h_i is the height of the i -th ball.

Only the robot’s fingertip is simulated in the simulation environment because, in the real-world environment, the robot’s kinematics do not affect the task achievement. The observations s are formatted in the same way as in the real-robot because the depth information can be accurately obtained in the simulation, and s^{depth} is directly assigned as the simulation ball-height to each pixel without initializing the robot position. The definitions of actions a and rewards r are the same as in the real-world environment. The domain parameters used for DR and their ranges are shown in Table 4. This task randomizes the physical and sensor model’s parameters. Since balls in the real world are deformed by the robot’s physical interaction, making balls move in strange directions, parameters including ball-radius and friction-coefficient are randomized to express

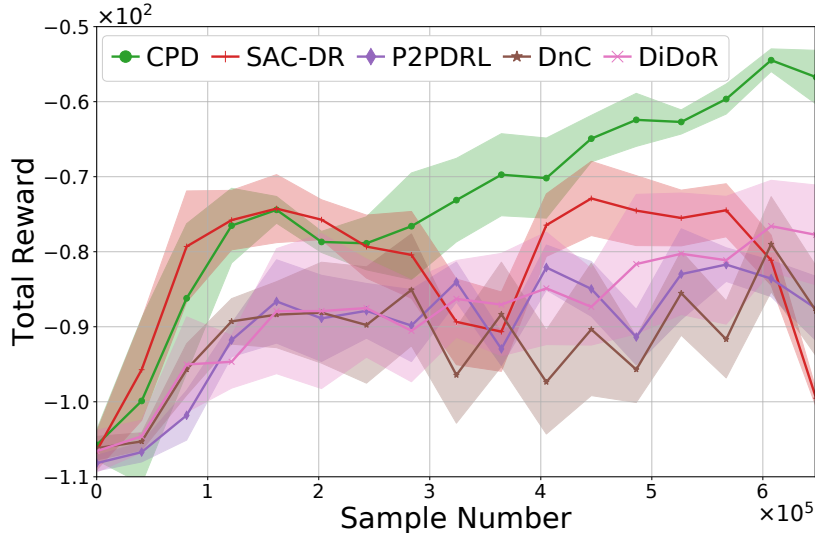


Figure 8: Learning curves of ball-dispersal task: Each curve plots mean and variance of total reward over five experiments.

this phenomenon. Furthermore, the depth sensor is so noisy that observations of depth images between simulation and the real world have huge gaps, and thus observations of ball positions and sizes are randomized by injecting noise. SAC updates local policies and local value functions as a base-RL method, with the same networks and setting as in Sec. 5.1. Due to the higher task difficulty compared to the simulation experiments, all node numbers of networks are increased to 128.

6.2. Results

CPD and other baselines are compared in Fig. 8. The convergence of SAC-DR is faster than CPD in the initial stage of training, but the performance soon becomes unstable. The top total reward of SAC-DR can be achieved by one touch to the balls. The balls then transition to an enormous number of patterns, and SAC-DR cannot find good actions under such conditions. On the other hand, CPD shows stable performance improvement and achieves around 40% better total reward than the other baselines.

To evaluate the effectiveness of the learned policies for sim-to-real transfer,




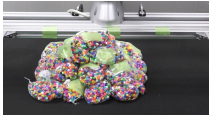


Method	SAC	SAC-DR	CPD
Final View (Juggling)			
Achieve	0 / 14	6 / 14	13 / 14
Final View (Beads)			
Achieve	0 / 14	1 / 14	11 / 14

Table 5: Task achievement of learned policies of ball-dispersal task: Final-view means the final result of evaluating policy actions in one episode. Achieve represents task achievement, assessed by the number of balls dropped on the floor. This experiment uses two types of balls: (1) juggling balls that are hard and easy to move and (2) bead balls that are easily deformed and difficult to move. This experiment uses 30 balls, with 16 balls first placed on the floor and the other 14 balls placed on the first 16 balls; here, the second set of 14 balls is used to evaluate task achievement. Each task achievement is evaluated over five experiments per each learned policy.

we prepared two test environments with different types of balls, juggling balls and bead balls. Table 5 shows the results of evaluating how well the balls can be collapsed using the learned policies from the experiments shown in Fig. 8. We also evaluate SAC trained without DR as a comparison. Just as SAC-DR could not achieve good performance in simulation, the method only collapsed about half of the balls in the real-world environment of juggling balls. Furthermore, SAC-DR could not collapse bead balls, which are more difficult than juggling balls. In fact, SAC could not even access the balls. In contrast, CPD could collapse almost all of the balls for both types of balls.

Fig. 9 shows snapshots of the simulation and the real-world environments with the learned CPD policy obtained in the experiment shown in Fig. 8. From the observation, the scale and noise of the balls’ position and depth information are different between the simulation and the real world. However, since the scale and noise of the balls’ position and depth information are widely randomized, the task is achieved by transferring the simulation policies to the real world in a zero-shot setting.

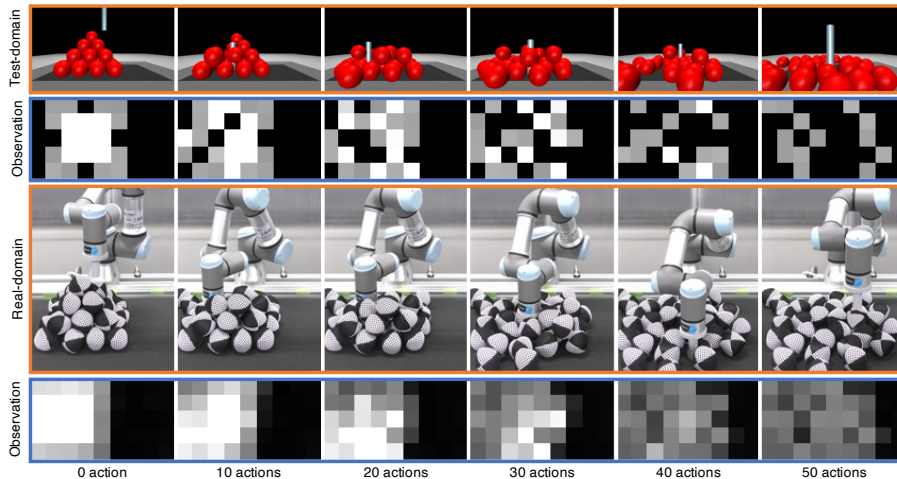


Figure 9: Snapshots of robot’s state and observation in the ball-dispersal task executed by the learned policy of CPD: Upper two rows are environments and observations of simulation. Lower two rows are environments and observations of real world. These observations are depth images compressed to (5,9). The simulation observations are randomized by DR as given in Table 4.

7. Discussion

In the current CPD framework, the dividing number N of the range of randomized parameters needs to be set manually. As described in Sec. 5.3, the dividing number N controls the tradeoff between the learning stability and the sample efficiency. Besides, three different partitioning patterns were considered for the proposed method, and their robustness to these patterns was confirmed. In common, they give equal importance to all sub-domains, but they may not all contribute equally for policy distillation. Developing a mechanism to identify sub-domains that do not contribute to learning and exclude them from periodic transitions is a future work.

Since CPD learns by cyclically transitioning through each sub-domain, it does not seem straightforward to extend it to parallelized RL [36, 37, 38]. However, CPD can indeed be extended to parallelized RL by grouping a certain number of sub-domains as one cluster. Such a method could be applied to larger domains.

The proposed method has an Actor-critic structure for RL. Therefore, the

proposed method requires policies and action value functions, and applicable learning algorithms include the latest DRL algorithms such as SAC, TD3 [39], and DDPG [40]. This paper utilizes SAC which is the best performance actor-critic method [33].

The experimental results indicated that our CPD could empirically achieve better sample efficiency than the previous methods for multiple tasks. However, its theoretical justification remains open since the theoretical guarantees of the original MI method were obtained assuming a single domain [27] and might not hold in a randomized environment.

8. Conclusion

In this paper, we proposed CPD as a sample-efficient RL method with DR for sim-to-real. The effectiveness of the method was demonstrated by experiments using both simulations and real-world tasks. The experimental results showed that CPD achieved higher performance and better sample efficiency than that of comparison methods.

Acknowledgments

This work is supported by JST Moonshot Research and Development, Grant Number JPMJMS2032.

References

- [1] V. Mnih, K. Kavukcuoglu, D. Silver, A. A. Rusu, J. Veness, M. G. Bellemare, A. Graves, M. Riedmiller, A. K. Fidjeland, G. Ostrovski, et al., Human-level control through deep reinforcement learning, *Nature* 518 (7540) (2015) 529–533.
- [2] S. Levine, P. Pastor, A. Krizhevsky, J. Ibarz, D. Quillen, Learning hand-eye coordination for robotic grasping with deep learning and large-scale data

- collection, *The International Journal of Robotics Research (IJRR)* 37 (4-5) (2018) 421–436.
- [3] S. Gu, E. Holly, T. Lillicrap, S. Levine, Deep reinforcement learning for robotic manipulation with asynchronous off-policy updates, in: *IEEE International Conference on Robotics and Automation (ICRA)*, 2017, pp. 3389–3396.
- [4] J. Tobin, R. Fong, A. Ray, J. Schneider, W. Zaremba, P. Abbeel, Domain randomization for transferring deep neural networks from simulation to the real world, in: *IEEE/RSJ International Conference on Intelligent Robots and Systems (IROS)*, 2017, pp. 23–30.
- [5] J. Matas, S. James, A. J. Davison, Sim-to-real reinforcement learning for deformable object manipulation, in: *Conference on Robot Learning (CoRL)*, 2018, pp. 734–743.
- [6] B. Mehta, M. Diaz, F. Golemo, C. J. Pal, L. Paull, Active domain randomization, in: *Conference on Robot Learning (CoRL)*, 2020, pp. 1162–1176.
- [7] C. Zhao, T. Hospedales, Robust domain randomised reinforcement learning through peer-to-peer distillation, in: *Asian Conference on Machine Learning (ACML)*, 2021, pp. 1237–1252.
- [8] Y. Sun, P. Fazli, Ensemble policy distillation in deep reinforcement learning, in: *Advancement of Artificial Intelligence (AAAI)*, 2020.
- [9] Y. Chebotar, A. Handa, V. Makoviychuk, M. Macklin, J. Issac, N. Ratliff, D. Fox, Closing the sim-to-real loop: Adapting simulation randomization with real world experience, in: *IEEE International Conference on Robotics and Automation (ICRA)*, 2019, pp. 8973–8979.
- [10] F. Muratore, C. Eilers, M. Gienger, J. Peters, Data-efficient domain randomization with bayesian optimization, *IEEE Robotics and Automation Letters (RA-L)* 6 (2) (2021) 911–918.

- [11] F. Ramos, R. C. Possas, D. Fox, Bayessim: adaptive domain randomization via probabilistic inference for robotics simulators, in: *Robotics: Science and Systems (RSS)*, 2019.
- [12] J. Brosseit, B. Hahner, F. Muratore, M. Gienger, J. Peters, Distilled domain randomization, arXiv preprint arXiv:2112.03149.
- [13] D. Ghosh, A. Singh, A. Rajeswaran, V. Kumar, S. Levine, Divide-and-conquer reinforcement learning, in: *International Conference on Learning Representations (ICLR)*, 2018.
- [14] G. Brockman, V. Cheung, L. Pettersson, J. Schneider, J. Schulman, J. Tang, W. Zaremba, Openai gym, arXiv preprint arXiv:1606.01540.
- [15] E. Todorov, T. Erez, Y. Tassa, Mujoco: A physics engine for model-based control, in: *IEEE/RSJ International Conference on Intelligent Robots and Systems (IROS)*, 2012, pp. 5026–5033.
- [16] C. Matl, Y. Narang, R. Bajcsy, F. Ramos, D. Fox, Inferring the material properties of granular media for robotic tasks, in: *IEEE International Conference on Robotics and Automation (ICRA)*, 2020, pp. 2770–2777.
- [17] S. Clarke, T. Rhodes, C. G. Atkeson, O. Kroemer, Learning audio feedback for estimating amount and flow of granular material, *Proceedings of Machine Learning Research (PMLR)* 87.
- [18] N. Tuomainen, D. Blanco-Mulero, V. Kyrki, Manipulation of granular materials by learning particle interactions, *IEEE Robotics and Automation Letters (RA-L)* 7 (2) (2022) 5663–5670.
- [19] D. Jud, P. Leemann, S. Kerscher, M. Hutter, Autonomous free-form trenching using a walking excavator, *IEEE Robotics and Automation Letters (RA-L)* 4 (4) (2019) 3208–3215.
- [20] P. Egli, D. Gaschen, S. Kerscher, D. Jud, M. Hutter, Soil-adaptive excavation using reinforcement learning, *IEEE Robotics and Automation Letters (RA-L)*.

- [21] Q. Lu, Y. Zhu, L. Zhang, Excavation reinforcement learning using geometric representation, *IEEE Robotics and Automation Letters (RA-L)* 7 (2) (2022) 4472–4479.
- [22] A. A. Rusu, S. G. Colmenarejo, Ç. Gülçehre, G. Desjardins, J. Kirkpatrick, R. Pascanu, V. Mnih, K. Kavukcuoglu, R. Hadsell, Policy distillation, in: *International Conference on Learning Representations (ICLR)*, 2016.
- [23] S. Stanton, P. Izmailov, P. Kirichenko, A. A. Alemi, A. G. Wilson, Does knowledge distillation really work?, *Neural Information Processing Systems (NeurIPS)* 34 (2021) 6906–6919.
- [24] Y. W. Teh, V. Bapst, W. M. Czarnecki, J. Quan, J. Kirkpatrick, R. Hadsell, N. Heess, R. Pascanu, Distral: Robust multitask reinforcement learning, in: *Neural Information Processing Systems (NeurIPS)*, 2017, pp. 4499–4509.
- [25] R. T. Kalifou, H. Caselles-Dupré, T. Lesort, T. Sun, N. Diaz-Rodriguez, D. Filliat, Continual reinforcement learning deployed in real-life using policy distillation and sim2real transfer, in: *International Conference on Machine Learning (ICML)*, 2019, pp. 4497–4507.
- [26] S. Omidshafiei, J. Papis, C. Amato, J. P. How, J. Vian, Deep decentralized multi-task multi-agent reinforcement learning under partial observability, in: *International Conference on Machine Learning (ICML)*, 2017, pp. 2681–2690.
- [27] S. Kakade, J. Langford, Approximately optimal approximate reinforcement learning, in: *International Conference on Machine Learning (ICML)*, 2002, pp. 267–274.
- [28] Y. Abbasi-Yadkori, P. L. Bartlett, S. J. Wright, A fast and reliable policy improvement algorithm, in: *International Conference on Artificial Intelligence and Statistics (AISTATS)*, 2016, pp. 1338–1346.

- [29] M. Pirotta, M. Restelli, A. Pecorino, D. Calandriello, Safe policy iteration, in: International Conference on Machine Learning (ICML), 2013, pp. 307–315.
- [30] N. Vieillard, O. Pietquin, M. Geist, Deep conservative policy iteration, in: Association for the Advancement of Artificial Intelligence (AAAI), 2020, pp. 6070–6077.
- [31] L. Zhu, T. Kitamura, M. Takamitsu, Cautious actor-critic, in: Asian Conference on Machine Learning (ACML), 2021, pp. 220–235.
- [32] W. M. Czarnecki, R. Pascanu, S. Osindero, S. Jayakumar, G. Swirszcz, M. Jaderberg, Distilling policy distillation, in: International Conference on Artificial Intelligence and Statistics (AISTATS), 2019, pp. 1331–1340.
- [33] T. Haarnoja, A. Zhou, P. Abbeel, S. Levine, Soft actor-critic: Off-policy maximum entropy deep reinforcement learning with a stochastic actor, in: International Conference on Machine Learning (ICML), 2018, pp. 1861–1870.
- [34] X. B. Peng, M. Andrychowicz, W. Zaremba, P. Abbeel, Sim-to-real transfer of robotic control with dynamics randomization, in: IEEE International Conference on Robotics and Automation (ICRA), 2018, pp. 3803–3810.
- [35] J. Schulman, F. Wolski, P. Dhariwal, A. Radford, O. Klimov, Proximal policy optimization algorithms, arXiv preprint arXiv:1707.06347.
- [36] A. Nair, P. Srinivasan, S. Blackwell, C. Alcicek, R. Fearon, A. De Maria, V. Panneershelvam, M. Suleyman, C. Beattie, S. Petersen, et al., Massively parallel methods for deep reinforcement learning, arXiv preprint arXiv:1507.04296.
- [37] V. Mnih, A. P. Badia, M. Mirza, A. Graves, T. Lillicrap, T. Harley, D. Silver, K. Kavukcuoglu, Asynchronous methods for deep reinforcement learning, in: International Conference on Machine Learning (ICML), 2016, pp. 1928–1937.

- [38] D. Horgan, J. Quan, D. Budden, G. Barth-Maron, M. Hessel, H. van Hasselt, D. Silver, Distributed prioritized experience replay, in: International Conference on Learning Representations (ICLR), 2018.
- [39] S. Fujimoto, H. Hoof, D. Meger, Addressing function approximation error in actor-critic methods, in: International Conference on Machine Learning (ICML), 2018, pp. 1587–1596.
- [40] T. P. Lillicrap, J. J. Hunt, A. Pritzel, N. Heess, T. Erez, Y. Tassa, D. Silver, D. Wierstra, Continuous control with deep reinforcement learning, in: International Conference on Learning Representations (ICLR) (Poster), 2016.